Journal of Quantitative Spectroscopy & Radiative Transfer 299 (2023) 108504

Contents lists available at ScienceDirect

Journal of Quantitative Spectroscopy & Radiative Transfer

journal homepage: www.elsevier.com/locate/jqsrt

The j and k dependencies of the line coupling and line mixing effects: Theoretical studies of the relaxation matrices of N_2-broadened CH_3D

Q. Ma [a,*], C. Boulet [b]

[a] NASA/Goddard Institute for Space Studies and Department of Applied Physics and Applied Mathematics, Columbia University, 2880 Broadway, New York, NY 10025, USA

[b] Institut des Sciences Moléculaires d'Orsay (ISMO), CNRS. Université Paris-Saclay, Bât. 520, Campus d'Orsay 91405 Orsay-CEDEX, France

ARTICLE INFO

Article history:
Received 6 January 2023
Revised 22 January 2023
Accepted 23 January 2023
Available online 24 January 2023

Keywords:
Methane-d
N_2 broadened CH_3D line shape
Line coupling and line mixing
Infant health
Semi-classical line shape theory

ABSTRACT

Line coupling and line mixing effects in parallel and perpendicular bands of CH_3D perturbed by N_2 have been studied. The work focuses on exhibiting the j and k dependencies of these two processes. The calculations were based on a previously reported anisotropic intermolecular potential including both the long-range multipole, induction, and dispersion forces and a short-range atom-atom model. It is shown that components with $L_1 = 3$ of the atom-atom model are dominant contributions to the diffusion operator. As a consequence, in comparison with other molecular systems such as the CH_3Cl-N_2 and CH_3I-N_2, theoretically predicted line coupling and line mixing effects exhibit completely new j and k dependencies. In general, the theoretically calculated halfwidths and intra-doublets' off-diagonal elements of the relaxation matrix are in reasonable agreement with measurements.

1. Introduction

Accurate lineshape parameters of monodeuterated methane CH_3D are crucial for quantitative analyses of the spectral signatures of this molecule in the terrestrial and other planetary atmospheres (see Ref. [1] and references therein). This is the reason why numerous studies have been devoted both experimentally and theoretically to the halfwidths (HWHM) and shifts of air- as well as self- broadened lines in various vibrational bands (a complete review can be found in [2–5]).

From the theoretical point of view, which concerns us most directly, the most recent calculations of N_2 broadened halfwidths of CH_3D lines have been performed by Predoi-Cross et al. [4,5] based on the Robert-Bonamy (RB) formalism [6] using exact trajectories and a potential model including an atom-atom potential model.

In recent papers devoted to N_2-broadening of symmetric top molecules [7–9], we have shown that the isolated line approximation severely limits the validity of the RB model. As outlined previously by Cherkasov [10], the S_2 operator is not diagonal in the linespace, contrary to the isolated line assumption adopted in the RB model [11]. Ignoring this fact (called by us as Line Coupling (LC)) leads to neglecting any coupling between transition lines and a failure in calculating the relaxation matrix. For symmetric tops with k-degeneracy, LC will have an additional consequence: transitions between rotational states labeled by $k \neq 0$ should be considered as doublets. For each doublet, its two components are coupled through the line mixing (LM) process. For degenerated doublets (i.e. not resolved by the A_1-A_2 splitting), the LM process may significantly reduce theoretically calculated halfwidths of the doublet.

The present work is devoted to the CH_3D-N_2 system. For its degenerate doublets, we have found that the intra-doublet's coupling does play a major role in the calculation of the halfwidths. However, for CH_3D a significant A_1-A_2 splitting exists (for states in the fundamental vibrational state, with $k = 3n$, $n = 1, 2, 3, \ldots$). Consequently, the degeneracy of the corresponding doublets can be resolved, providing an opportunity to directly measure the intra-doublet's off-diagonal elements of the relaxation matrix. Then, the latter can be compared with the theoretical predictions.

2. Theory

2.1. A short background

Within the binary collision and impact approximations, the spectral density at the angular frequency ω can be written as

Abbreviations: HWHM, Halfwidth; RB, Robert-Bonamy; MRB, Modified Robert-Bonamy; RRB, Refined Robert-Bonamy; LC, Line Coupling; LM, Line Mixing; CSF, The Coupling Strength Factor; PES, Potential Energy Surface.

* Corresponding author.
E-mail address: qm2@columbia.edu (Q. Ma).

https://doi.org/10.1016/j.jqsrt.2023.108504
0022-4073/

[12,13]

$$F(\omega) = \frac{1}{\pi} Im \sum_{n,l} d_l \sqrt{\rho_l} \left\langle l \right| \frac{1}{\omega - L_0 - iPW} \left| n \right\rangle \sqrt{\rho_n} d_n \ , \quad (1)$$

where $|n\rangle \equiv |v_f j_f k_f \varepsilon_f;\ v_i j_i k_i \varepsilon_i\rangle$ are the Liouville vectors associated with the transition $v_f j_f k_f \varepsilon_f \leftarrow v_i j_i k_i \varepsilon_i$. A background of this basis set applicable for symmetric tops is given in Section 2 and in Appendix of Ref. [14]. In Eq. (1), $\rho_n = \frac{\exp(-\beta E_n)}{Z}$ are matrix elements of the density operator exclusive of the magnetic degeneracy and Z is the partition function, $E_n = E(v_i j_i k_i \varepsilon_i)$ is the initial energy of transition, and d_n is the associated transition dipole operator. Finally, W is the symmetrized relaxation matrix.

After removing the isolated line approximation assumed both in the RB formalism and in the MRB formalism defined later, one is able to calculate the matrix elements of W with an expression given by

$$W_{f'i',fi} = \frac{n_b \bar{v}}{2\pi c} \int_{r_{c,min}}^{+\infty} 2\pi b \left(\frac{db}{dr_c} \right) \left\{ \delta_{i'i} \delta_{f'f} - \ll f'i' \left| e^{-S_2(r_c)} \right| fi \gg \right\} dr_c, \quad (2)$$

where n_b is the number density of the bath molecules, $\bar{v}$ is the mean relative speed, b is the impact parameter, and r_c is the closest distance of approach for a given collisional trajectory. We note that in Eq. (2), an average over the collisional kinetic energy is replaced by the mean relative speed.

In Eq. (2), because S_2 is a non-diagonal operator in the linespace, $\ll f'i'|e^{-S_2(r_c)}|fi\gg \neq e^{-\ll f'i'|S_2(r_c)|fi\gg}$ whose effect is called by us as line coupling (LC). The general expressions of the various contributions to S_2 (outer-i, outer-f, and middle) are given in Refs. [15,16]. Remember that the non-diagonality of S_2 solely results from the $S_{2,middle}$ term which is given in Eq. (1) of Ref. [17].

Then, as we evaluate the spectral density from Eq. (1), we introduce another terminology of line mixing (LM) resulting from the non-diagonality of the resolvent operator of $(\omega - L_0 - iPW)^{-1}$. In this case, each of the eigenvectors of $L_0 - iPW$ is given by a combination of different lines. In other words, these eigenvectors lead to line mixing. At this stage, as one compares theoretically calculated halfwidths with measurements, depending on the absorber's spectrum characters and perturber's pressure P, one needs to choose a proper way to consider the LM effect.

For symmetric-top molecules, when the A_1-A_2 splitting is insignificant between the two components of a doublet and for E-E transitions which are also degenerate doublets (provided that $k_{i\,orf} \neq 0$), the situation is similar. At low perturber's pressures, various doublets are isolated from each other and the treatment of the resolvent operator is limited to the corresponding 2×2 linespace. In the following, we will denote two coupled components of a doublet by 1 and 2. In addition, we will denote $\langle 1|W|1\rangle = \langle 2|W|2\rangle$ for the diagonal elements and $\langle 1|W|2\rangle = \langle 2|W|1\rangle$ for the intra-doublet's off-diagonal ones. The frequency detuning (i.e., line splitting) is $\omega_2 - \omega_1 = 2\Delta\omega > 0$. Therefore, following a method proposed by Ben Reuven [18], the effective halfwidth of an "isolated" doublet is the sum of the diagonal and off-diagonal elements, i.e., $W(1,1) + W(1,2)$ (assuming equal intensities between the two components) [7,8]. Since $W(1,2)$ is negative, $W(1,1) + W(1,2)$ is less than $W(1,1)$. For CH_3D, in some cases as compared to a model ignoring the k degeneracy, it may reduce the halfwidths up to 20–30% as shown later. When the A_1-A_2 splitting is resolved, both $W(1,1)$ and $W(1,2)$ can be measured independently. In this case, $W(1,1)$ and $W(1,2)$ represent theoretically calculated halfwidth and coupling element.

For readers' convenience, we outline the developing stages of our formalism here.

(1) The modified Robert-Bonamy (MRB) formalism. In this early version of our formalism, the expression for halfwidth γ is given by

$$\gamma_{fi} = \frac{n_b \bar{v}}{2\pi c} \int_{r_{c,min}}^{+\infty} 2\pi b \left(\frac{db}{dr_c} \right) \left\{ 1 - e^{-\ll fi|S_2(r_c)|fi\gg} \right\} dr_c, \quad (3)$$

where a subtle derivation error in the RB formalism had been corrected by the current authors [12]. The essential difference between RB and MRB is the definition of S_2 whether it excludes or includes the bath average procedure. Besides this, they don't differ much. Usually, calculated halfwidths with MRB are slightly larger than those obtained with RB. Because both RB and MRB are based on the isolated line approximation, with these two formalisms one is not able to calculate the whole relaxation matrix W.

(2) The refined Robert-Bonamy (RRB) formalism where the invalid isolated line approximation has been removed and LC is taken into account. As shown in Eq. (2), with this model one is able to calculate the relaxation matrix W in which the diagonal elements are calculated halfwidths.

(3) The most updated formalism applicable for symmetric-top molecules with complete k degeneracy. Besides LC, with this model the LM effect resulting from evaluating the resolvent operator and the spectral density has been taken into account. For a doublet, the effective halfwidth of a doublet becomes $W(1,1) + W(1,2)$, where $W(1,1) \equiv W^{RRB}_{f_1 i_1, f_1 i_1} = W^{RRB}_{f_2 i_2, f_2 i_2}$ and $W(1,2) \equiv W^{RRB}_{f_1 i_1, f_2 i_2} = W^{RRB}_{f_2 i_2, f_1 i_1}$. For the A-A transitions with significant A_1-A_2 splitting, a detailed discussion is given later (see Section 3.3.3).

2.2. The interaction potential

For systems consisting of a symmetric-top and a linear molecule, the potential can be expressed in terms of a spherical tensor expansion as (cf. Eq. (5) of Ref. [15] and reference therein)

$$V\left(\vec{R}(t)\right) = \sum_{L_1 K_1 L_2} U(L_1 L_2 L; K_1 K_2 = 0; R(t)) \times \sum_{\mu_1 \mu_2 M} C(L_1 L_2 L, \mu_1 \mu_2 M) D^{L_1 *}_{\mu_1 K_1}(\Omega_1) D^{L_2 *}_{\mu_2 0}(\Omega_2) Y^*_{LM}(\omega(t)). \quad (4)$$

With respect to the anisotropic part of the potential, we have retained the potential model together with its parameters and the cut-offs detailed in Predoi-Cross et al. [4]. It is expressed as a sum of the multipole, induction and dispersion forces completed by an atom-atom interaction model. All the parameters are given in Tables 3 and 4 of Ref. [4]. The cut-offs used by them are $L_1 = 3$ and $L_2 = 2$ for the multipole interaction and the atom-atom interaction. Meanwhile $L_1 = 2$ and $L_2 = 2$ for the induction and dispersion forces. Note that since CH_3D has a very small electric dipole and a zero electric quadrupole moment and the diatomic molecule N_2 has a zero electric dipole, the multipole interactions between CH_3D and N_2 are extremely weak. On the other hand, the induction and dispersion forces only have no-zero and weak components associated with $L_1 = 2$ and $L_1 = 1$, respectively. Thus, components of the atom-atom interaction become dominated ones and make major contributions to matrix elements of S_2. In Fig. 1 we show the various components $U(L_1 L_2 L;\ 00;\ R)$ of this potential model. It is obvious that components with $L_1 = 3$ (i.e., 303, 321, 323, 325) are the dominant ones. In comparison with CH_3I-N_2 studied by us previously [9], due to the weakness of the long-range interactions of CH_3D-N_2, it becomes necessary to add the atom-atom model here. In addition, in the present study, following the choice made by Predoi-Cross et al. [4], the cut-off of L_1 is extended from 2 to 3. As shown later, this extension leads to new features of LC and LM variation patterns. Finally, since all the components

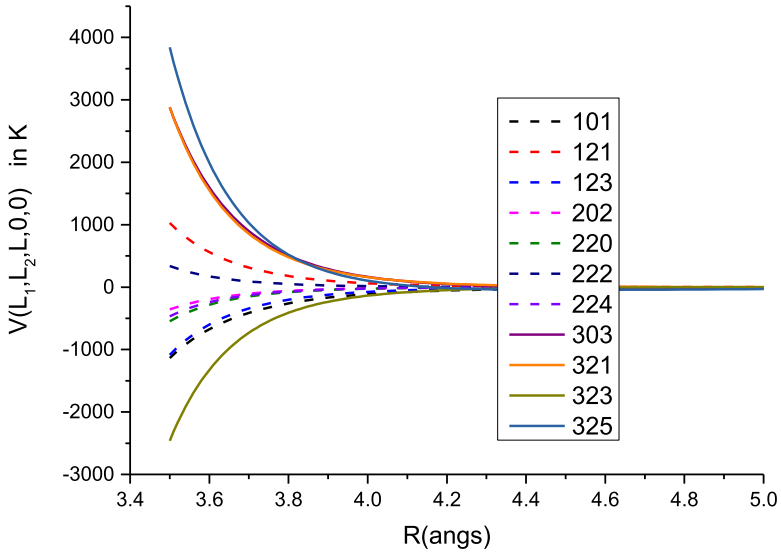

Fig. 1. Potential spherical components (in the units of K) considered in the present study.

of the anisotropic potential correspond to $K_1 = 0$, LC and LM only exist between lines belonging to the same sub-branch specified by their initial and final k values.

As usual, we assume that the collisional trajectories are only determined by the isotropic part of potential. To be more consistent, the latter should be the component $U(000; 00; R)$ divided by $\sqrt{4\pi}$. In Ref. [4] it has been firstly fitted by the Lennard-Jones (LJ) model. Then, these authors slightly optimized its parameters to improve agreement between their calculated halfwidths with the RB formalism and measurements. However, by using their LJ parameters (i.e., $\varepsilon = 83.50$ K and $\sigma = 3.838$ Å), we can't obtain a reasonable agreement with the data. This was well expected because in comparison with the RB formalism, our formalism, by considering the effects from both LC and LM, yields significantly different results. In facing such a situation, there are two choices available.

We could try to adjust all the atom-atom parameters and the cut-offs to reach the best agreement with data. However, such a tedious procedure will be heavy to implement [19,20]. Alternatively, with exactly sticking to the current anisotropic potential parameters and the cut-offs, one can keep the LJ model for the isotropic part and optimize its two parameters [21].

Because the main purpose of the present study is to exhibit and explain the j and k dependencies of LC and LM effects of CH_3D-N_2, rather than to produce more accurate results, we have decided to adopt the second choice. The temperature considered in the present calculations is the room temperature T = 296 K. After taking an optimizing procedure, the isotropic LJ potential is given by $\varepsilon = 110$ K and $\sigma = 3.68$ Å. We note that the two LJ parameters of CH_4-N_2 derived from the fitting viscosity data by Bastien et al. [22] are 130.1 K and 3.675 Å which are close to our values.

In the present study, the energy levels and the line frequencies of CH_3D were taken from the HITRAN 2020 data base [23].

3. Results and discussion

3.1. Line coupling strength factor

In our previous studies, we have found that the off-diagonal elements of S_2 are mainly determined by the coupling strength factor (CSF) with the rank L_1 and the two arguments of the two-dimensional Fourier transforms with the rank L_1 and L_2 [15]. It is known that both LC and LM result from the non-diagonality of S_2. Therefore, in order to analyze the j and k dependencies of LC and LM, one needs to focus on these two factors. For the intra-doublet's off-diagonal elements of S_2, the expression for CSF is simplified as

$$(-1)^{L_1}(2j_f+1)(2j_i+1)W(j_ij_fj_ij_f,\,1L_1)D^p(\varepsilon_i' j_i k_i,\,\varepsilon_i j_i k_i;\,L_1 0)D^p(\varepsilon_f' j_f k_f,\,\varepsilon_f j_f k_f;\,L_1 0), \tag{5}$$

where $W(j_ij_fj_ij_f, 1L_1)$ is the Wigner 6j symbol and D^p matrix is defined in Eq. A(3) of Ref. [15]. We note that within a doublet the choice of the index of ε is fixed, CSF becomes a function of L_1, j_f, k_f, j_i, and k_i. In addition, for a specified sub-branch, values of j_f and k_f are determined by j_i and k_i. Therefore, CSF is a function of L_1, j_i and k_i. On the other hand, the two arguments of the Fourier transforms are the frequency and energy gaps (cf. Eq. (1) of Ref. [17]) and can be easily derived from the energy levels of CH_3D and N_2. For the intra-doublet's off-diagonal elements of S_2, the frequency gap is zero or almost zero. As for the energy gap it consists of the active and bath molecular contributions. For the former, it is zero or almost zero. For the latter, due to carrying out the bath average, its effect does not vary as the line of interest varies. In summary, as one analyzes the j and k dependencies of LC and LM, one can neglect the role played by the second factor.

In Fig. 2, we present the functions of CSF with $L_1 = 1$ and 3 noted as CSF(1) and CSF(3). As shown in the figure, the variation pattern of CSF(1) is well organized. As j increases, the magnitude of CSF(1) decreases. Meanwhile, as k increases, the magnitude increases. The increasing paces of k for low j doublets are faster than higher j ones. In contrast, the variation pattern of CSF(3) is completely different and becomes more complicated. In general, as j increases, the magnitudes increase first and reach their maximum, then decrease. For doublets with $k \geq 3$, there are structures for low j values. With respect to the k dependence of CSF(3), the variation pattern is complicated for $j < 16$. After $j \geq 16$, as k increases, the magnitude increases.

From Fig. 1, one already knows that the potential components with $L_1 = 3$ are dominating. Given the fact that the one- and two-dimensional Fourier transforms labeled by L_1 and L_2 are associated with products of the potential components with the same ranks, the dominant role of CSF(3) would be squared in evaluating the off-diagonal elements of S_2. Thus, one can conclude that variation patterns of LC and LM should be somehow similar to its pattern.

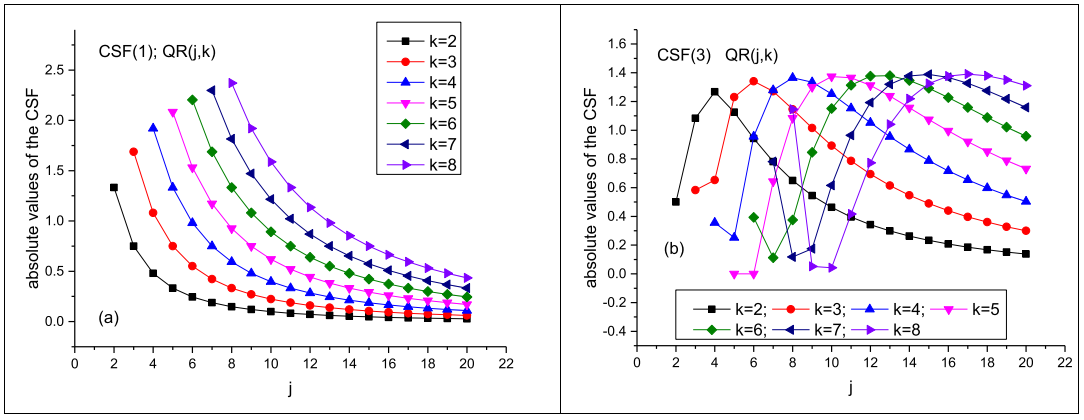

Fig. 2. Calculated lines coupling strength factors (CSF) with $L_1 = 1$ and 3.

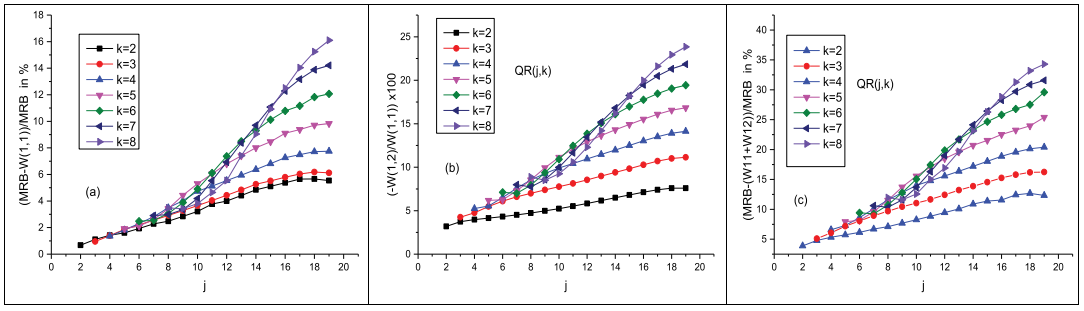

Fig. 3. Calculated relative reductions resulting from considering LC, LM, and LC+LM. They are presented in Figs. 3a, b, and c, respectively.

It is worth mentioning, the Fourier transforms with $L_1 = 2$ don't make contributions to the intra-doublet's off-diagonal elements of S_2. This claim results from the fact that these Fourier transforms are associated with CSF(2). Meanwhile, for the two lines in a doublet, their symmetry index assignments are opposite (i.e., $\varepsilon \cdot \varepsilon' = -1$). Thus, CSF(2) are zero because $D^P(\varepsilon' jk, \varepsilon jk; 20) = 0$ (cf. Eq. (12) of Ref [14]). Therefore, as one considers the intra-doublet's LC, one can completely neglect $L_1 = 2$. However, with respect to LM things are subtly different. The Fourier transforms with $L_1 = 2$ do make contributions to the inter-doublet's off-diagonal elements of S_2. Consequently, through the diagonalization and integration procedures appearing in Eq. (2), they slightly play a role in calculations of the intra-doublet's off-diagonal elements of W.

3.2. The j and k dependencies of LC and LM

After completing our discussions on CSF, we present some of our theoretically calculated results. According to the value of k_i, the doublets of CH_3D are divided into the E-E ($k_i \neq 3n$) and A-A ($k_i = 3n$) transitions. The A-A transitions consist of two categories: without and with A_1-A_2 significant splitting. From a theoretical point of view, the doublets belonging to E-E transition and A-A transition without A_1-A_2 splitting have a complete k-degeneracy. Those belonging to the A-A transitions with a significant A_1-A_2 splitting don't have such k-degeneracy. We have used the three versions of our formalism to complete calculations. They are simply labeled as MRB, RRB, and RRB+LM later or alternatively as without LC, with LC, and with LC+LM.

Based on our experiences in studying other molecules, we know that in comparison with a calculated halfwidth with MRB, RRB reduces it by a certain amount, then RRB+LM reduces it further. In order to clearly show the importance of effects from the LC, LM, and LC+LM and also their j and k dependencies, we present relative reductions of halfwidth in the ν_6 band due to considering LC, LM and LC+LM in Figs. 3a, 3b, and 3c, respectively. For simplicity, we neglect the subscript i in j and k. As shown in Fig. 3a, the effect of LC depends on k and j, varying from less than 2% for $k \leq 5$ and $j \leq 5$ and more than 10% for $k \geq 6$ and $j \geq 16$. The maximum reduction reaches 16% at $k = 8$ and $j = 19$. Note that in general, as j increases, the reduction increases as well. But, in regions with low j values, they may not be monotonic functions. As functions of k, the above claim is also true. These features are well expected because they result from the structure of CSF(3) mentioned previously. Meanwhile as shown in Fig. 3b, the reduction pattern of LM is somehow similar to LC, but becomes stronger. It varies from less than 10% for $k \leq 6$ and $j \leq 8$ and more than 20% for $k \geq 7$ and $j \geq 16$. The maximum reaches 24% at $k = 8$ and $j = 19$. In addition, a non-monotonic behavior appears again. Finally, the j and k dependencies and the whole effect of LC+LM become the strongest as shown in Fig. 3c. The reductions are more than 27% for $k \geq 7$ and $j \geq 16$ and the maximum reaches 34% at $k = 8$ and $j = 19$.

It is worth mentioning that for other systems (i.e., CH_3Cl-N_2 and CH_3I-N_2) studied by us previously [8,9], we have found a "usual" behavior where the relative reduction is a monotonic function of j_i and k_i. As j_i increases it decreases and as k_i increases it increases. Meanwhile, effects from LC, LM, and LC+LM reach the maximum in the vicinity of $j_i \approx k_i$. In fact, due to relatively strong long-range interactions occurring in these systems, the cut-off used in studying these systems was $L_1 = 2$ and $L_2 = 2$. As a result, their simple features directly result from the profile of CSF(1) shown in Fig. 2a. In fact, we have made a test by using the same cut-off $L_1 = 2$ and $L_2 = 2$ for CH_3D-N_2. Of course, in this case calculated halfwidths become too low to match measurements. But, the reduction feature becomes "usual", similar to CH_3Cl-N_2 and CH_3I-N_2.

In summary, we have exhibited a new feature of the j and k dependencies for the CH_3D-N_2 system and provided a clear explanation about where they come from and why they happen. Our conclusion is that because CH_3D-N_2 has a very weak long-range

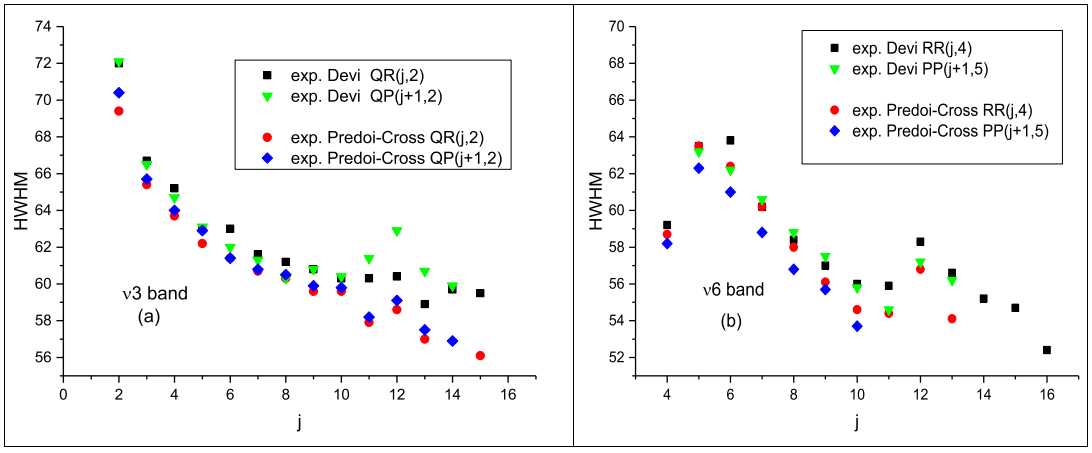

Fig. 4. Verifications of the symmetry properties for some measured halfwidths (in the units of 10^{-3}cm^{-1}atm^{-1}) in the ν_3 and ν_6 bands. They are presented in Figs. 4a and b, respectively.

interaction, one must add the atom-atom model and the latter's components with $L_1 = 3$ lead to totally different rotational dependencies of the LC and LM processes.

3.3. Comparisons with measurements

With respect to measurements, the most recent N_2-broadening data were obtained by Malathy Devi et al. [2,3] and Predoi-Cross et al. [4,5] for the ν_3 parallel band and the ν_5 and ν_6 perpendicular ones, using FTS spectroscopy. In these experiments, $T = 296$ K and the N_2 pressure varies from 100 Torr to 400 Torr (Devi) and 600 Torr (Predoi-Cross). All recorded spectra were simultaneously fit using a multi-spectrum non-linear least square procedure detailed in Ref. [4]. For some selected pairs of transitions (corresponding to A_1-A_2 resolved doublets), both the $W(1,1)$ and $W(1,2)$ matrix elements were also determined.

3.3.1. Some symmetry considerations

Due to the very weak or zero vibrational dependence of both the rotational constants driving the collisional transitions and of the average values of the molecular parameters in the initial and final vibrational levels, some symmetry properties may be established from theoretical predictions. For instance, one can easily demonstrate a series of equalities between calculated halfwidths (with and without LC and LM). Such as

$$QR(j,k) \approx QP(j+1,k) \text{ in parallel bands,} \tag{6a}$$

$$RR(j,k) \approx PP(j+1,k+1) \text{ in perpendicular bands.} \tag{6b}$$

The weak or no- vibrational dependence of both the rotational and molecular parameters has another consequence: a negligible vibrational dependence of the relaxation matrices. Then, as already noted in Ref. [4], calculations made in the ν_6 band can be used in analyzing the ν_5 band.

We have checked if the experimental data by Devi and by Predoi-Cross in the ν_3 band obey Eq. (6a). For this purpose we have considered all the QR(j,k) and QP(j + 1,k) pairs for k = 1, 2, 4, 5, 6, 7, 8. In general, Eq. (6a) was well verified and the measurements by these two teams only differ slightly. However in some cases, significant differences appear at high j. For $j < 10$, as shown in Fig. 4a, both their measurements in sub-branches with $k = 2$ remain at the 1% accuracy level and differences of their data are about 2%. However, for $j > 10$, the data of Devi fails to satisfy Eq. (6a) at the same level and exhibit a "bump" as j increases. In the ν_6 band (Fig. 4b) the results are quite similar and for small j the difference between data in the ν_6 and ν_5 bands (not shown here) often differ slightly. But here too, for high j the measured j variation pattern looks strange. In our opinion, the scattered distributions appearing at high j should be related to a great difficulty in measuring and also in fitting parameters within congested spectra.

3.3.2. The E-E transition and the A-A transition without A_1-A_2 splitting

First of all, we consider the E-E transition and the A-A transition without A_1-A_2 splitting in the ν_3 band and present comparisons between calculated results and measurements in Fig. 5. The sub-branches selected are QP(j, k) with k = 2, 4, 5, and 6 and QR(j,k) with k = 2, 4, 6, and 8. The theoretical results consist of calculated halfwidths without LC (i.e., MRB), with LC (i.e., RRB), and with LM (i.e., RRB+LM). The measurements are by Predoi-Cross et al. [5] and by Malathy et al. [3]. As shown in Fig. 5, in comparison with the two earlier stages, our results with RRB+LM are closer to the measurements and in general, the agreement with the measured values is reasonable. Meanwhile, with these figures one can easily find gaps resulting from using different versions of our formalism. These gaps represent the effects from LC and LM and their variation patterns show the j and k dependencies of LC and LM. It is obvious that the variation patterns of gaps in the QR sub-branch are consistent with that described above in Fig. 3. With respect to the QR and QP sub-branches, Fig. 5 shows these features are also applicable.

Then, we consider the E-E transition and the A-A transition without A_1-A_2 splitting in the ν_6 and ν_5 perpendicular bands. As mentioned above, calculations made in the ν_6 band can be used in analyzing the ν_5 band. In Fig. 6, we present comparisons between calculated results and measurements in the ν_6 and ν_5 bands. The sub-branches selected are PQ(j,k) with k = 2, 4, 5, 6 and RR(j,k) with k = 4, 5, 6, 8. In general, the explanations of Fig. 5 are also applicable here and we don't repeat them again. However, it is worth carefully looking at the j and k dependencies of the halfwidths in the RR(j,k) sub-branches given in Fig. 6e–h. One observes a significant dip of the halfwidths happening at $j_i = k_i$ and the dip becomes larger as k_i increases. Although the most updated model correctly predicts these dips, it quantitatively fails at reproducing their depths. Meanwhile, the agreement between calculated and observed halfwidths becomes poorer as the k increases. Nevertheless, one can conclude that for symmetric top molecules, the correct treatment of the k-degeneracy is absolutely necessary. In addition, in order to improve the agreements, a refinement of the current atom-atom model is required.

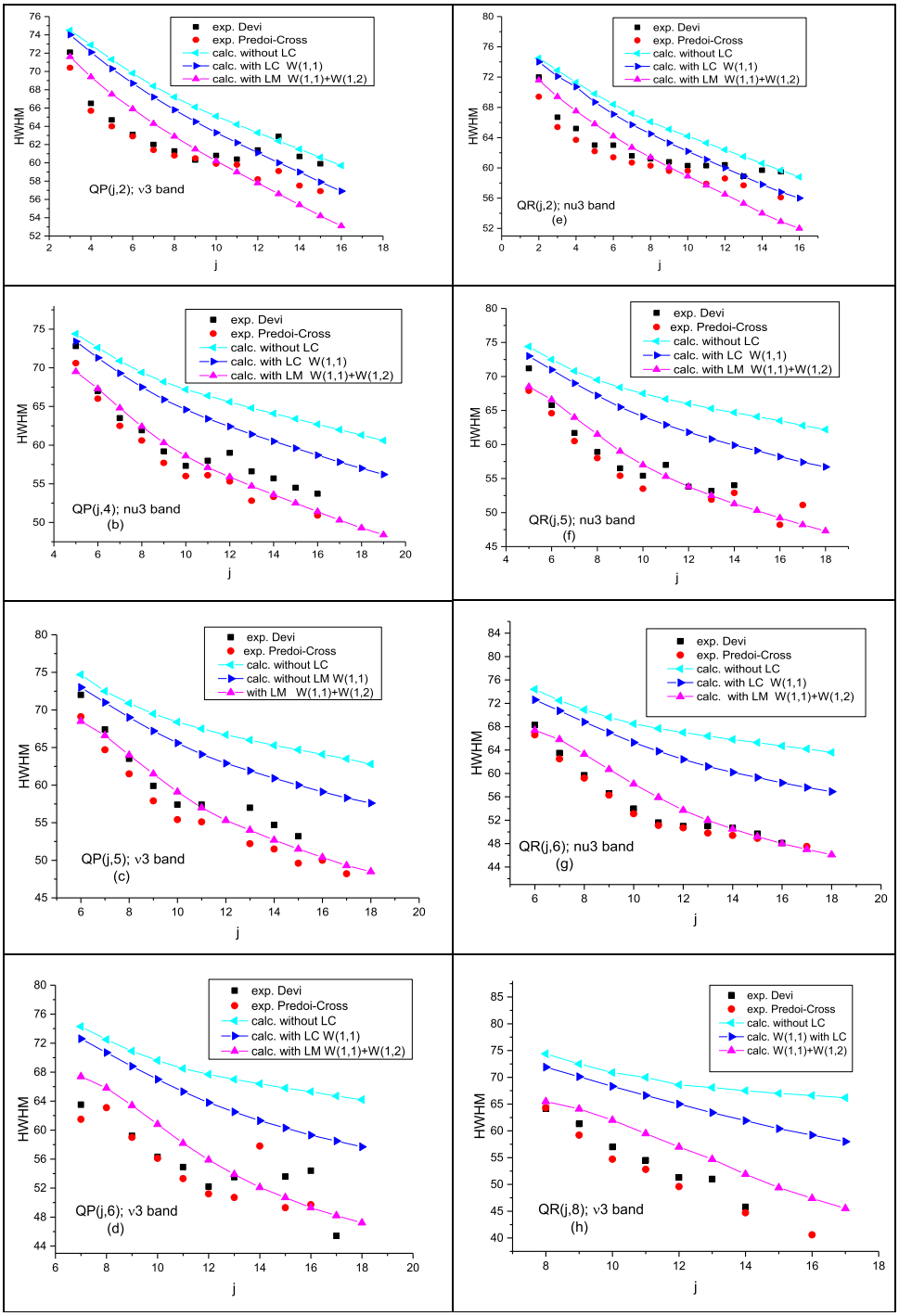

Fig. 5. Comparisons between calculated halfwidths and measurements (in the units of 10^{-3}cm^{-1}atm^{-1}) in the ν_3 band. The calculations are made with three different methods: MRB, RRB, and RRB+LM. The sub-branches considered are QP(j,k) with k = 2, 4, 5, 6 and QR(j,k) with k = 2, 4, 6, 8. These results are presented in Figs. 5(a)–(d) and Figs. 5(e)–(h), respectively.

3.3.3. The A-A transitions with A_1-A_2 splitting

The intra-doublet off-diagonal elements $W(1,2)$ have been measured, only for some doublets belonging to sub-branches with $k_i = 3$. As is well known, the inversion of the experimental profiles should be adapted to the experimental conditions. If a splitting is insignificant, i.e. $2\Delta\omega \ll \gamma$, whatever the perturber's pressure, the situation is somehow similar to that discussed in III-3b. Here we are concerned with a case of "partially" resolved doublet. A doublet belongs to that category if $2\Delta\omega \geq \gamma$ for almost all the pressure range. As is well known from our previous studies [7], in such a situation, both $W(1,1)$ and $W(1,2)$ could be independently measured (assuming that the doublet remains isolated from its neighbors belonging to the same sub-branch).

However, the situation is not clear in the ν_3 band: no line mixing effects have been obtained from the fittings by Malathy et al. [3]. On the opposite, weak line mixing effects have been observed by Predoi-Cross et al. [5] for some doublets in the QP(j,3) and QR(j,3) sub-branches. Their observed intra-doublet's matrix elements are listed in Table 1.

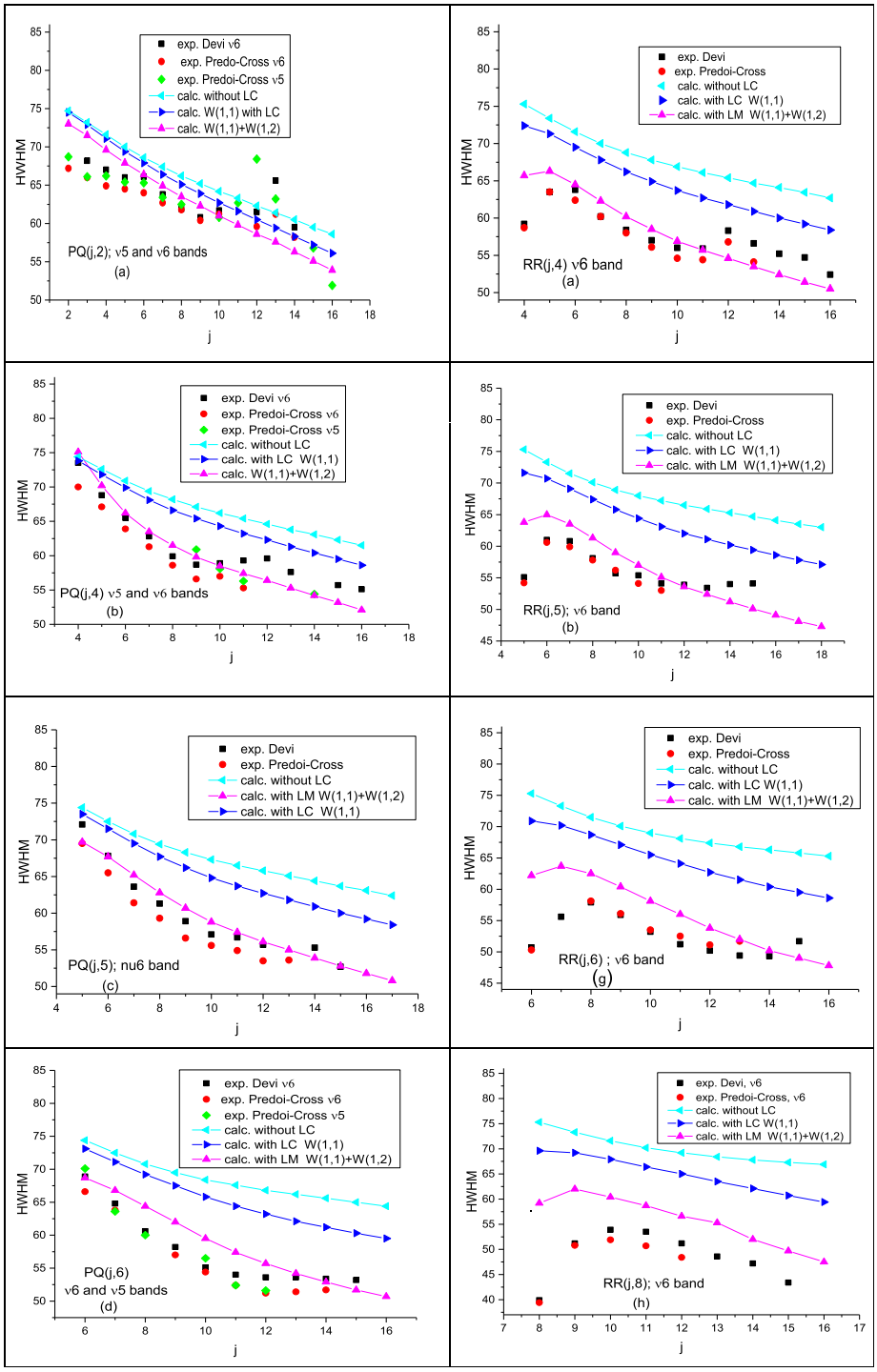

Fig. 6. The same as Fig. 5 except for in the ν_6 and ν_5 bands and the sub-branches are PQ(j,k) with k = 2, 4, 5, 6 and RR(j,k) with k = 4, 5, 6, 8. These results are presented in Figs. 6(a)–(d) and Figs. 6(e)–(h), respectively.

Table 1
Intra-doublet's matrix elements (10^{-3}cm^{-1}atm^{-1}) of QP(j,3) and QR(j,3) in the ν_3 band.

doublet	$-W(1,2)$ Exp. [5]	$W(1,1)$ Exp. [5]	$-W(1,2)$ Calc.	$W(1,1)$ Calc.	A_1-A_2 Splitting (10^{-3}cm^{-1})	Measurement is possible?
QP(10,3)	6.3	60.7	4.7	64.1	4.0	No
QP(11,3)	19.1	54.6	4.8	63.0	6.8	No
QP(12,3)	3.1	57.1	5.0	62.0	12.0	Yes
QR(7,3)	1.44	57.6	4.4	66.5	≈ 0	No
QR(11,3)	4.0	53.6	5.0	61.9	19.1	Yes
QR(12,3)	6.0	59.7	5.2	60.9	29.4	Yes

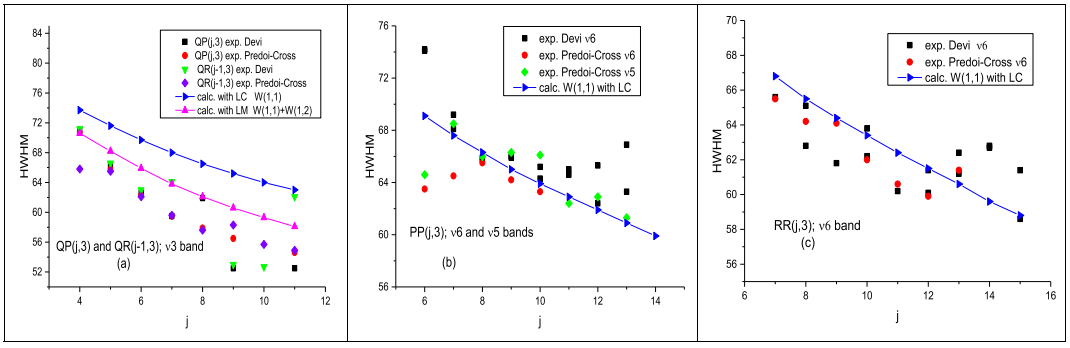

Fig. 7. Comparisons between calculated halfwidths and measurements (in the units of $10^{-3}cm^{-1}atm^{-1}$) for sub-branches in the ν_3, ν_6, and ν_5 bands. These results are presented in Figs. 7a, b, and c, respectively.

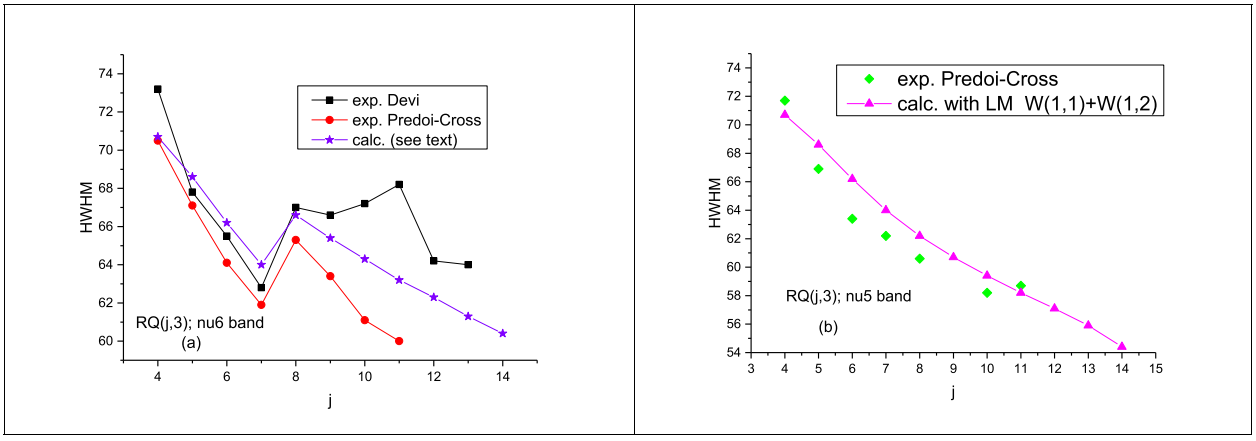

Fig. 8. Comparisons between theoretically calculated halfwidths and measurements of RQ(j,3) (in the units of $10^{-3}cm^{-1}atm^{-1}$) in the ν_6 and ν_5 bands. These results are presented in Figs. 8a and b, respectively.

Table 2
Intra-doublet's off-diagonal elements of $-W(1,2)$ ($10^{-3}cm^{-1}atm^{-1}$) in the PP(j,k) sub-branch.

PP(j,3)	Predoi-Cross ν_5 [5]	Predoi-Cross ν_6 [4]	Devi ν_6 [2]	Calc.
5	10.0	–	–	3.4
6	11.3	4.8	10.5	3.4
7	6.2	3.4	6.0	3.5
8	–	4.5	4.5	3.5
9	–	4.8	4.3	3.5
10	–	4.0	3.1	3.6

Table 3
Intra-doublet's off-diagonal elements of $-W(1,2)$ ($10^{-3}cm^{-1}atm^{-1}$) in the RR(j,k) sub-branch.

RR(j,3)	Devi ν_6 [2]	Predoi-Cross ν_6 [6]	Calc.
7	3.3	3.5	4.9
8	3.8	6.4	5.1
9	–	11.1	5.3
10	6.7	6.4	5.4
11	5.7	6.1	5.5
12	–	6.3	5.7
13	–	6.0	5.8
14	4.3	–	6.0
15	4.9	–	6.1

Knowing that a halfwidth of interest varies from about $8 \times 10^{-3}cm^{-1}$ to $32 \times 10^{-3}cm^{-1}$ when the pressure of N_2 varies from 100 to 400 Torr, it can be easily understood that for the three lines (labeled as "No"in the last column of Table 1), the experimental conditions do not allow one to make a conclusive measurement of both $W(1,1)$ and $W(1,2)$. This implies that in these cases (i.e., $j < 12$), the listed values of observed $W(1,1)$ and $W(1,2)$ are less meaningful and the measured halfwidths rather correspond to $W(1,1) + W(1,2)$. The comparison is given in Fig. 7a. As shown in the figure, the values of $W(1,1) + W(1,2)$ are closer to the measurements than $W(1,1)$. Note that the symmetry between QP($j + 1$,3) and QR(j,3) is also presented there.

Then, we consider measurements made in the ν_6 and ν_5 bands. In the PP(j,3) sub-branch, based on whether $2\Delta\omega \geq \gamma$ is satisfied or not, it is possible to measure the intra-doublet's off-diagonal elements $W(1,2)$ from $j = 6$ to 12 in the ν_6 band and for $j = 5$ to 7 in the ν_5 one. Table 2 gives a comparison of the calculated and measured $W(1,2)$, while Fig. 7b and c give the comparison between the measured and calculated diagonal elements $W(1,1)$. As shown in the figure and Table 2, the agreement is good.

Coupling elements have been also measured in the RR(j,3) sub-branch of the ν_6 band. Since the splitting varies from 44 to $14 \times 10^{-3}cm^{-1}$ for $7 \leq j \leq 15$, it was indeed possible to separately measure W(1,1) and $W(1,2)$. Table 3 shows a comparison between calculated and observed elements $-W(1,2)$, while Fig. 7c shows the comparison between the observed halfwidths and $W(1,1)$. Here too the agreement may be considered as reasonable.

Finally, we consider a more interesting situation: that of the RQ(j,3) sub-branch. In the ν_6 band, the splitting is insignificant for $j \leq 7$ [2,4,23] ($2\Delta\omega = 5.4 \times 10^{-3}cm^{-1}$ for $j = 7$), then it suddenly goes to 44×10^{-3} cm^{-1} for $j = 8$ and remains important up to $j = 13$ (i.e., $37 \times 10^{-3}cm^{-1}$). Meanwhile, the splitting in the ν_5 band remains insignificant whatever the j values [5,23]. Consequently, all the measurements in the ν_5 band correspond to $W(1,1) + W(1,2)$. The situation in the ν_6 band is more complex. For $j \leq 7$, they still correspond to $W(1,1) + W(1,2)$. In contrast, they correspond to $W(1,1)$ for $j \geq 8$ because it has been possible to measure

Table 4
Intra-doublet's off-diagonal elements of $-W(1,2)$ (10^{-3}cm^{-1}atm^{-1}) in the RQ(j,3) sub-branch.

RQ(j,3)	Devi ν_6 [2]	Calc.
8	4.9	4.2
9	6.3	4.7
10	6.1	4.9
11	4.1	5.0
12	2.3	5.2
13	4.4	5.4

both $W(1,1)$ and $W(1,2)$. In Fig. 8, we present comparisons between our calculated halfwidths in the sub-branch of RQ(j,3) in the ν_6 and ν_5 bands and the corresponding measurements. Note that the theoretical values are obtained with the way explained above. As shown in Fig. 8a, our theoretical result correctly explains a sudden "jump" observed between $j = 7$ and 8 both by Devi et al. and Predoi-Cross et al.. Meanwhile, as shown in Fig. 8b, both our result, i.e. $W(1,1) + W(1,2)$ and the measurement in the ν_5 band don't exhibit any "jump" at all. Table 4 gives the corresponding comparison between the coupling elements. Of course more reliable data are required to corroborate that analysis.

4. Conclusions

Overall the calculated halfwidths and intra-doublet's off-diagonal elements are in reasonable agreement with the available experimental data. Meanwhile, the present study contains some weaknesses. Besides the well-known weaknesses inherent in current semi-classical line shape formalisms, others include:

(1) The use of simple symmetric top wavefunctions. More accurate wavefunctions may be obtained from a tensorial formalism [24] allowing one to take into account the various resonances existing between the vibrational bands of this spectral region.
(2) The deficiency of the atom-atom potential model used in the present study. As expected, the accuracy of the short-range interaction is of crucial importance for that system. Going further requires the need of more refined potential energy surfaces (PES). As mentioned previously, a coherent adjustment of the atom-atom parameters (i.e. including both the isotropic and anisotropic parts of the potential in the optimizing procedure) should be a solution. For CH_3D-N_2, an alternative exists: recent ab-initio PES for CH_4-N_2 have been reported ([25] and references therein). Its implementation in calculating the relaxation matrix remains a challenge but represents, in our opinion, a next step in the analysis of LC and LM processes in the CH_3D-N_2 system.

However, our simplified approach has allowed one to exhibit new interesting features for CH_3D-N_2. The dominant short-range interaction between CH_3D and N_2 contains predominant anisotropic components with $L_1 = 3$. It turns out that these components play a dominant role in calculating the halfwidths and relaxation matrices W. In addition, it is these components that cause a completely different j and k dependencies of the line coupling and the line mixing.

Finally, mainly due to the lack of measured matrix elements of $W(1,2)$ and the large uncertainties involved, it is difficult to make experimental verifications of the theoretically predicted j and k dependencies of LC and LM. More reliable measurements are required. At the same time, spectra recorded at much higher perturber's pressures will be useful to check other calculated off-diagonal elements of W (i.e. inter-doublet off-diagonal elements) [26].

Declaration of Competing Interest

The authors declare that they have no known competing financial interests or personal relationships that could have appeared to influence the work reported in this paper.

CRediT authorship contribution statement

Q. Ma: Conceptualization, Methodology, Formal analysis, Data curation, Writing – original draft, Writing – review & editing. **C. Boulet:** Conceptualization, Methodology, Formal analysis, Data curation, Writing – original draft, Writing – review & editing.

Data availability

Data will be made available on request.

Acknowledgment

The authors would like to thank the reviewer for improving the manuscript. One of the authors (i.e., Q. Ma) acknowledges support from the NASA Radiation Sciences Program managed by Hal Maring. This research used resources of the National Energy Research Scientific Computing Center, which is supported by the Office of Science of the U.S. Department of Energy under Contract No. DE-AC02-05CH11231.

References

[1] Buldyreva J, Lavrentieva NN, Dudaryonok AS. Semi-empirical calculations of line-shape parameters and their temperature dependences for parallel bands of monodeuterated methane perturbed by nitrogen. JQSRT 2017;203:355–66.
[2] Malathy Devi V, Benner DC, Brown LR, Smith MAH, Rinsland CP, Sams RL, Sharpe SW. Multispectrum analysis of self- and N_2-broadening in the ν_6 band of $^{12}CH_3D$. JQSRT 2002;72:139–91.
[3] Malathy DV, Benner DC, Smith MAH, Rinsland CP, Brown LR. Multispectrum analysis of self- and nitrogen-broadening, pressure shifting and line mixing in the ν_3 parallel band of $^{12}CH_3D$. JQSRT 2002;73:603–40.
[4] Predoi-Cross A, Malathy DV, Sung K, Sinyakova T, Buldyreva J, Benner DC, Smith MAH, Mantz AW. Temperature dependences of N_2-broadening and shift coefficients in the ν_6 perpendicular band of $^{12}CH_3D$. JQSRT 2015;163:120–41.
[5] Predoi-Cross A, Malathy DV, Sutradhar P, Sinyakova T, Buldyreva J, Sung K, Smith MAH, Mantz AW. Temperature dependences of self- and N_2-broadened line-shape parameters in the ν_3 and ν_5 bands of $^{12}CH_3D$. JQSRT 2016;177:181–215.
[6] Buldyreva J, Guinet M, Eliet S, Hindle F, Mouret G, Bocquet R, Cuisset A. Theoretical and experimental studies of CH_3X–Y_2 rotational line shapes for atmospheric spectra modelling: application to room-temperature CH_3Cl-O_2. PCCP 2011;13:26–34.
[7] Boulet C, Ma Q. Line shape parameters of PH_3 transitions: theoretical studies of self-broadened widths and line mixing effects. J Chem Phys 2020;152:214305.
[8] Ma Q, Boulet C. Theoretical study of CH_3Cl-N_2 line shapes in the ν_1 band. Line mixing effects in QR doublets and QQk sub-branches. JQSRT 2021;273:107844.
[9] Boulet C, Ma Q. Line coupling and line mixing effects on calculated widths of symmetric top molecules with the k-degeneracy: a theoretical study of N_2-, O_2- and air-broadened lines of CH_3I. JQSRT 2022;288:108273.
[10] Cherkasov MR. Theory of relaxation parameters of the spectrum shape in the impact approximation.I-General consideration. JQSRT 2014;141:73–88.
[11] Robert D, Bonamy J. Short-range force effects in semiclassical molecular line broadening calculations. J Phys 1979;40:923–43 (Paris).
[12] Ma Q, Boulet C, Tipping RH. Refinement of the Robet-Bonamy formalism: Considering effects from the line coupling. J Chem Phys 2013;139:034305.
[13] Boulet C, Ma Q, Thibault F. Line interference effects using a refined Robert-Bonamy formalism: the test case of the isotropic Raman spectra of N_2. J Chem Phys 2014;140:084310.
[14] Ma Q, Boulet C, Tipping RH. Relaxation matrix for symmetric tops with inversion symmetry. Line coupling and line mixing effects on NH_3 lines in the ν_4 band. J Chem Phys 2017;146:134312.
[15] Ma Q, Boulet C. The relaxation matrix for symmetric tops with inversion symmetry. I. Effects of line coupling on self-broadened ν_1 and pure rotational bands of NH_3. J Chem Phys 2016;144:224303.
[16] Boulet C, Ma Q. The relaxation matrix for symmetric tops with inversion symmetry. II. Line mixing effects in the ν_1 band of NH_3. J Chem Phys 2016;144:224304.
[17] Ma Q, Boulet C, Tipping RH. Vibrational dependence of line coupling and line mixing in self-broadened parallel bands of NH_3. JQSRT 2017;203:425–33.

[18] Ben-Reuven A. Impact broadening of microwave spectra. Phys Rev 1966;145:7–22.
[19] Gamache RR, Lamouroux J, Laraia AL, Hartmann JM, Boulet C. Semiclassical calculations of half-widths and line shifts for transitions in the 30012←00001 and 30013←00001 bands of CO_2 I: collisions with N_2. JQSRT 2012;113:976–90.
[20] Vispoel B, Cavalcanti JH, Gamache RR. Modified complex Robert-Bonamy calculations of line shape parameters and their temperature dependence for water vapor in collision with N_2. JQSRT 2019;228:79–89.
[21] Buldyreva J, Rohart F. Experimental and theoretical studies of room-temperature submillimetre $CH_3{}^{35}Cl$ line shapes broadened by H_2. Mol Phys 2012;110(17):2043–53.
[22] Bastien LAJ, Price PN, Brown NJ. Intermolecular parameters and combining rules determined from viscosity data. Int J Chem Kinet 2010;42:713–23.
[23] Gordon IE, et al. The HITRAN2020 molecular spectroscopic database. JQSRT 2022;277:107949.
[24] Nikitin A, Champion JP, Tyuterev V, Brown LR, Mellau G, Locke M. The infrared spectrum of CH_3D between 900 and 3200 cm^{-1}: extended assignment and modeling. J. Molec Structure 2000;517-518:1–24.
[25] Finenko AA, Chistikov DN, Kalugina YN, Conway EK, Gordon IE. Fitting potential energy and induced dipole surfaces of the van der Waals complex CH_4-N_2 using non-product quadrature grids. PCCP 2021;23:18475.
[26] Hadded S, Thibault F, Flaud PM, Aroui H, Hartmann JM. Experimental and theoretical study of line mixing in NH_3 spectra. II. Effect of the perturber in infrared parallel bands. J Chem Phys 2004;120:217–23.